

# Causal Representations of Neutron-Star Equations of State

Lee Lindblom

Center for Astrophysics and Space Sciences, University of California at San Diego, La Jolla, CA 92093, USA

(Dated: June 27, 2018)

Parameterized representations of the equation of state play an important role in efforts to measure the properties of the matter in the cores of neutron stars using astronomical observations. New representations are presented here that are capable of representing any equation of state to any desired level of accuracy, while automatically imposing causality and thermodynamic stability constraints. Numerical tests are presented that measure how accurately and efficiently these new parameterizations represent a collection of causal nuclear-theory model equations of state.

PACS numbers: 26.60.Kp, 26.60.-c, 26.60.Dd, 97.60.Jd

## I. INTRODUCTION

The equation of state describes the relationship between the total energy density  $\epsilon$ , the pressure  $p$ , the temperature  $T$ , and any other variables that determine the thermodynamic state of the material in a fluid. In newly formed neutron stars the extremely hot matter is expected to evolve quickly to its lowest energy state through high energy particle interactions; and the temperature of this material is expected to drop well below the Fermi temperature on a fairly short timescale through neutrino and photon emissions. Under these conditions the equation of state rapidly becomes almost barotropic, i.e. the energy density depends essentially only on the pressure of the material:  $\epsilon = \epsilon(p)$ .

The density of most of the material in a neutron star is larger than that of the matter in an atomic nucleus. Such densities are well beyond those accessible to laboratory experiments. Heavy ion scattering experiments (such as those carried out at RHIC and LHC) provide important information about the interactions between the various particles that make up neutron-star matter [1]. However those experiments can not duplicate the low temperature (i.e. well below the Fermi temperature) but very high density equilibrium conditions that exist in neutron stars.

In contrast to the dearth of directly relevant experimental data, a great deal of theoretical work has been done using the available data to construct models of neutron-star matter. Unfortunately there is no consensus at present on *the* correct model. This is not surprising, given the significant differences between neutron-star matter and the better understood matter contained in atomic nuclei. In particular, complicated many body interactions are likely to play an extremely important role in determining the properties of the cold very dense neutron-star matter. Figure 1 illustrates 34 published equations of state,  $\epsilon = \epsilon(p)$ , for neutron-star matter based on a variety of nuclear theory models.<sup>1</sup> This fig-

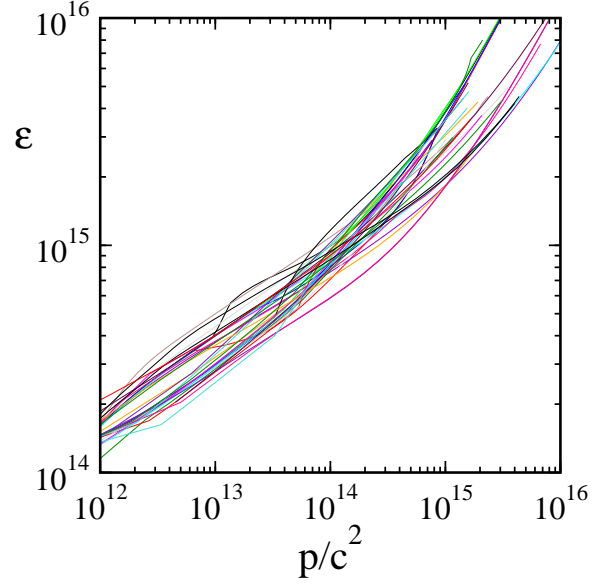


FIG. 1: Curves illustrate 34 nuclear-theory models of the neutron-star equation of state,  $\epsilon = \epsilon(p)$ . The density  $\epsilon$  and pressure  $p$  (divided by the speed of light squared) are displayed here in cgs units,  $\text{g}/\text{cm}^3$ .

ure illustrates the lack of consensus among the various models: at a given density,  $\epsilon$ , the associated value of the pressure varies by almost an order of magnitude.

Given the lack of direct laboratory access to neutron-star matter and the lack of consensus theoretical modeling for this material, observations of neutron stars may turn out to be the most promising way to obtain quantitative information about the equation of state of neutron-star matter. It is well known that the equation of state together with the gravitational field equations determine the structures and hence all the observable macroscopic properties of neutron stars [3]. Conversely, it is also

<sup>1</sup> The 34 equations of state shown in Fig. 1 are those used by Read, et al. [2] in their study of the piecewise-polytropic representations of neutron-star equations of state. The abbreviated names

of these equations of state are: PAL6, SLy, APR1, APR2, APR3, APR4, FPS, WFF1, WFF2, WFF3, BBB2, BPAL12, ENG, MPA1, MS1, MS2, MS1b, PS, GS1, GS2, BGN1H1, GNH3, H1, H2, H3, H4, H5, H6, H7, PCL2, ALF1, ALF2, ALF3. ALF4.

known that a complete knowledge of an appropriate set of macroscopic properties (e.g. masses and radii) together with the gravitational field equations uniquely determines the equation of state [4, 5]. Studies of neutron-star models have shown that their macroscopic properties, like masses and radii, vary widely even within the current “realistic” class of equations of state [2, 6]. Observations of the macroscopic properties of these stars would therefore provide significant constraints on the equation of state. Unfortunately the needed observations are quite difficult to make. Masses of several dozen neutron stars have now been measured fairly accurately (see e.g. Ref. [7]). These observations alone rule out large classes of very “soft” equation of state models that fail to support sufficiently massive neutron stars. A number of radius measurements of neutron stars have also been made [8–22]. At present these radius measurements are not nearly as accurate as the best mass observations, but hopefully the quantity and quality of these observations will continue to improve over time.

Good simultaneous measurements of both the mass and the radius (or some other macroscopic observable like the tidal deformability or the moment of inertia) are needed to determine the equation of state quantitatively from observations of neutron stars. Given a suitable set of observations,  $M_i$  and  $R_i$  (for example), the equation of state can be determined in the following way. First, a parametric representation of possible equations of state,  $\epsilon = \epsilon(p, \lambda_k)$ , is chosen. Next, stellar models are constructed using this parametric equation of state, and the associated observables,  $M(\lambda_k)$  and  $R(\lambda_k)$ , are evaluated for these models. Finally, the parameters  $\lambda_k$  are adjusted to optimally match the model observables,  $M(\lambda_k)$  and  $R(\lambda_k)$ , with the actual observations,  $M_i$  and  $R_i$ . The resulting equation of state,  $\epsilon = \epsilon(p, \lambda_k)$ , with this optimal choice of  $\lambda_k$  is an approximate representation of the physical neutron-star equation of state.

The approach outlined above for determining the equation of state has been tested using mock observational data constructed from the nuclear-theory model equations of state [4, 5, 23–25]. These tests show that accurate measurements of observables from a small number (just two or three) neutron stars can determine the high density part of the equation of state in the cores of neutron stars at the few percent accuracy level. Several groups have used qualitatively similar methods to estimate the actual neutron-star equation of state with the currently available (fairly inaccurate) observational data [9, 12, 20, 26–30].

This paper studies one important technical aspect of the method outlined above for determining the neutron-star equation of state: how to choose an appropriate parametric representation  $\epsilon = \epsilon(p, \lambda_k)$ . Several basic principles inform this choice:

1. Any equation of state should be representable by some  $\epsilon = \epsilon(p, \lambda_k)$  to any desired level of accuracy.
2. Each  $\epsilon = \epsilon(p, \lambda_k)$  should satisfy the basic laws of

physics, like thermodynamic stability and causality.

3. The representation should be efficient.

Since the neutron-star equation of state is not well understood at this time, it would not be appropriate to restrict its possible form with a non-universal representation. Principle #1 ensures that this does not happen. Whatever the neutron-star equation of state turns out to be, we can be quite confident that it will satisfy the basic laws of physics like thermodynamic stability and causality. Principle #2 requires that each parametric representation satisfies these conditions. And finally Principle #3 states the practical need for efficient parametric representations, i.e. those capable of achieving good accuracy with the fewest number of parameters possible. Fixing two parameters experimentally to achieve a certain level of accuracy with an efficient parameterization, for example, is much better than needing to fix four parameters to achieve the same level of accuracy using a less efficient parameterization.

Previous efforts to construct suitable representations of the neutron-star equation of state satisfy some, but not all of these principles. The widely used piecewise-polytropic representations [2, 31, 32] satisfy Principle #1, and the thermodynamic stability part of Principle #2, but they are not particularly efficient. The spectral representations [33] are more efficient, and they also satisfy Principle #1, and the thermodynamic stability part of Principle #2. None of the published representations enforce causality.

The main goal of this paper is to introduce and test new representations that satisfy all of the principles described above, including in particular the causality condition. Section II reviews the derivations of representations that satisfy Principle #1, and the thermodynamic stability part of Principle #2. Section III presents generalizations of these methods that find representations enforcing the simple causality condition appropriate for true barotropic equations of state. Section IV expands these discussions to include enthalpy-based representations that are the analogs of the pressure-based representations discussed in Secs. II and III. Section V tests the accuracy and efficiency of the various representations considered here (including the previously published forms) by constructing and measuring the accuracy of representations of 27 causal nuclear-theory model equations of state, the causal subset of those studied by Read, et al. [2]. And finally Sec. VI gives a brief summary and discussion of the most interesting and important results.

## II. THERMODYNAMICALLY STABLE REPRESENTATIONS

Thermodynamic stability requires that the energy density  $\epsilon$  must be a non-negative and monotonically increasing function of the pressure:  $\epsilon(p_1) \geq \epsilon(p_0) \geq 0$

for  $p_1 \geq p_0 \geq 0$ . For sufficiently differentiable equations of state, this is equivalent to the condition that  $d\epsilon/dp \geq 0$ . Every (sufficiently differentiable) equation of state  $\epsilon = \epsilon(p)$  determines a unique adiabatic index  $\Gamma(p)$ ,

$$\Gamma(p) = \frac{\epsilon(p) + p}{p} \left[ \frac{d\epsilon(p)}{dp} \right]^{-1}, \quad (1)$$

and thermodynamic stability therefore requires  $\Gamma(p)$  to be non-negative:  $\Gamma(p) \geq 0$ . Conversely every non-negative function  $\Gamma(p)$  determines a unique (up to a constant of integration) equation of state  $\epsilon = \epsilon(p)$  that satisfies the thermodynamic stability condition. This equation of state is the solution of the ordinary differential equation

$$\frac{d\epsilon(p)}{dp} = \frac{\epsilon(p) + p}{p\Gamma(p)}. \quad (2)$$

The problem of constructing representations of the equation of state,  $\epsilon(p)$ , is therefore equivalent to the problem of constructing representations of  $\Gamma(p)$ .

Physically acceptable representations of the adiabatic index  $\Gamma(p)$  are easier to construct than representations of the equation of state  $\epsilon(p)$  itself. Acceptable  $\epsilon(p)$  are more restrictive: they must be non-negative and monotonically increasing, while the  $\Gamma(p)$  need only be non-negative. Two different approaches have been used to construct appropriate representations of  $\Gamma(p)$ . The first constructs piecewise-analytical approximations for  $\Gamma(p)$ , which can be made arbitrarily accurate using a sufficiently large number of parameters. The piecewise-polytropic representations [2, 31, 32] are an example of this approach. The other approach constructs a spectral representation of  $\log \Gamma(p)$ , which can also be made arbitrarily accurate by including a sufficient number of terms in the expansion. An example of this approach [33] is a representation of  $\log \Gamma(p)$  as polynomials in  $\log p$ .

The basic idea of the piecewise-analytical representations is to use simple analytical functions  $\Gamma(p, \gamma_k)$  to represent  $\Gamma(p)$  on each of  $n$  subdomains,  $p_k \leq p < p_{k+1}$ , of the pressure domain of interest,  $p_0 \leq p \leq p_{\max}$ . The piecewise-polytropic representations are a particularly simple example. In this case the functions  $\Gamma(p, \gamma_k)$  are taken simply to be non-negative constants in each interval:  $\Gamma(p, \gamma_k) = \Gamma(p_k) = \gamma_k \geq 0$  for  $p_k \leq p < p_{k+1}$ . Any  $\Gamma(p)$  can clearly be approximated to any desired degree of accuracy in this way by using a sufficiently large number of pressure subdomains.

Once a particular representation  $\Gamma = \Gamma(p, \gamma_k)$  is chosen, it is straightforward to recover the underlying equation of state  $\epsilon = \epsilon(p, \gamma_k)$  by solving Eq. (2). As shown in Ref. [33] the solution to this equation can be reduced to quadratures:

$$\epsilon(p) = \frac{\epsilon_0}{\mu(p)} + \frac{1}{\mu(p)} \int_{p_0}^p \frac{\mu(p')}{\Gamma(p')} dp', \quad (3)$$

where  $\mu(p)$  is defined as

$$\mu(p) = \exp \left[ - \int_{p_0}^p \frac{dp'}{p' \Gamma(p')} \right], \quad (4)$$

and where  $\epsilon_0 = \epsilon(p_0) \geq 0$  is the constant of integration needed to fix the solution. For the simple piecewise-polytropic representation these integrals can be done analytically, and the equation of state  $\epsilon(p, \gamma_k)$  has the very simple analytical form,

$$\epsilon(p, \gamma_k) = \left( \epsilon_k - \frac{p_k}{\gamma_k - 1} \right) \left( \frac{p}{p_k} \right)^{1/\gamma_k} + \frac{p}{\gamma_k - 1}, \quad (5)$$

in the domain where  $p_k \leq p \leq p_{k+1}$ . The constants  $\epsilon_k$  are determined by the recursion relations

$$\epsilon_{k+1} = \left( \epsilon_k - \frac{p_k}{\gamma_k - 1} \right) \left( \frac{p_{k+1}}{p_k} \right)^{1/\gamma_k} + \frac{p_{k+1}}{\gamma_k - 1} \quad (6)$$

that enforce continuity of  $\epsilon(p, \gamma_k)$  at the subdomain boundaries.

The basic idea of spectral representations is to express functions as linear combinations of a complete set of basis functions, e.g.  $\Gamma(p) = \sum_k \gamma_k \Phi_k(p)$ . Physically acceptable  $\Gamma(p)$  must be non-negative, so unfortunately straightforward spectral expansions of  $\Gamma(p)$  are not useful. Typical basis functions, like the trigonometric functions or the orthogonal polynomials, are oscillatory, therefore allowing  $\Gamma(p)$  to become negative for many choices of the  $\gamma_k$ . This problem can be avoided, however, by using the spectral expansion to determine  $\log \Gamma(p)$ :

$$\Gamma(p, \gamma_k) = \exp \left[ \sum_k \gamma_k \Phi_k(p) \right]. \quad (7)$$

Any complete set of basis functions  $\Phi_k(p)$  can be used. The functions  $\Gamma(p, \gamma_k)$  are automatically non-negative for any choice of  $\gamma_k$ ; and these representations can be made arbitrarily accurate simply by including enough terms in the expansion. As in the piecewise-analytical case, the equation of state  $\epsilon = \epsilon(p, \gamma_k)$  is recovered using Eqs. (3) and (4). While the integrals in these equations can not in general be done analytically, they can be done numerically very efficiently. The simple choice of basis functions  $\Phi_k(p) = [\log(p/p_0)]^k$  was tested and used in Ref. [33].

Figure 2 illustrates  $\Gamma(p)$  for the 27 causal nuclear-theory model neutron-star equations of state used as test examples in this paper. These equations of state include all those used by Read, et al. [2] in their study of the piecewise-polytropic representations, except the 7 which violate the causality condition  $dp/d\epsilon \leq c^2$  for some range of densities: APR2, APR3, APR4, WFF1, WFF2, ENG, and ALF1. The particular equations of state have not been identified with their corresponding curves in Fig. 2 (nor those in Figs. 3–7). This omission was motivated in part by practical considerations: there are simply too many closely spaced and overlapping curves to allow them

to be labeled clearly. Instead, the data presented in these figures is intended to give an overall impression in Figs. 2–4 of the range of variability in the nuclear-theory model equations of state, and an overall impression in Figs. 5–7 of the range of accuracies of the various representations studied here. The detailed discussion of how efficiently the piecewise-analytical (PB-PA) and the spectral (PB-S) representations<sup>2</sup> work for these various equations of state is delayed to Section V. However to summarize, those tests reveal that the spectral expansions are more efficient, but both approaches work surprising well given the complexity of the functions  $\Gamma(p)$  seen in Fig. 2.

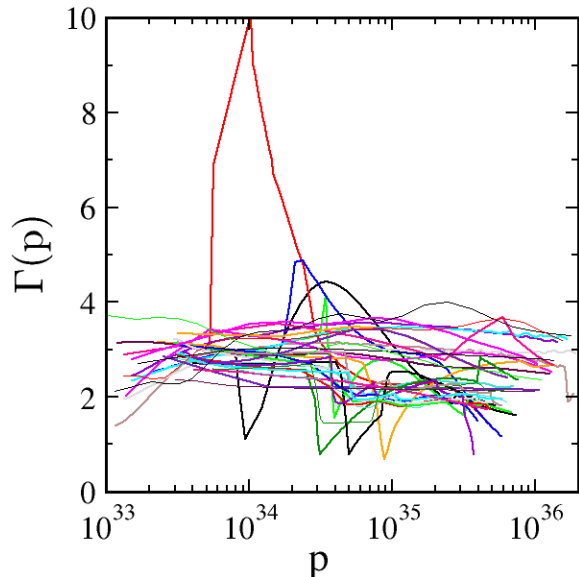


FIG. 2: Curves illustrate the adiabatic index  $\Gamma(p)$  for the 27 causal nuclear-theory model equations of state used to test the accuracy and efficiency of various parametric representations.

### III. CAUSAL REPRESENTATIONS

Sound waves propagate at the “characteristic” speeds of the hyperbolic equations that describe the evolution of a relativistic fluid. For a fluid having a true barotropic equation of state (i.e. one that is barotropic even for non-equilibrium fluid states), these characteristic speeds are related to the equation of state by the simple expression

$$v^2(p) = \left[ \frac{d\epsilon(p)}{dp} \right]^{-1}. \quad (8)$$

Causality, therefore, requires the equation of state for such fluids to satisfy the requirement  $d\epsilon(p)/dp \geq c^{-2}$ , where  $c$  is the speed of light.

Neutron-star matter is a complex mixture of many species of particles. There is a reasonably compelling argument that the equilibrium state of this material has a barotropic equation of state (see Sec. I). However the argument that the equation of state remains barotropic even for the non-equilibrium perturbations that propagate as sound waves is much less compelling.<sup>3</sup> The characteristic speeds of such complex mixtures will be determined by the detailed micro-physics that governs the dynamics of the mixture. Given the lack of a consensus nuclear-theory model for neutron-star matter, it is not surprising that the characteristic speeds and hence the causal properties of this material are not well understood at this time. Given this uncertainty, this paper simply adopts the (widely used but possibly irrelevant) causality condition for true barotropes:

$$\frac{d\epsilon(p)}{dp} = \frac{1}{v^2(p)} \geq \frac{1}{c^2}. \quad (9)$$

The goal in this section is to construct parametric representations of the equation of state that automatically enforce all of the principles outlined in Sec. I, including causality. Thermodynamic stability is equivalent to the condition that the sound speed squared,  $v^2(p)$ , is non-negative. This condition, together with the causality condition given in Eq. (9), implies that any physical equation of state must have sound speeds that satisfy,  $0 \leq v^2(p) \leq c^2$ . It is convenient to impose both the causality and the thermodynamic stability conditions as a single inequality on the function  $\Upsilon(p)$ :

$$\Upsilon(p) = \frac{c^2 - v^2(p)}{v^2(p)} \geq 0. \quad (10)$$

The function  $\Upsilon(p)$  plays much the same role in causal representations as the adiabatic index  $\Gamma(p)$  played in the discussion of the thermodynamically stable representations of the equation of state in Sec. II. Like the adiabatic index,  $\Upsilon(p)$  must be non-negative,  $\Upsilon(p) \geq 0$ . Like the adiabatic index, every (sufficiently differentiable) equation of state  $\epsilon = \epsilon(p)$  determines a unique  $\Upsilon(p)$ . And like the adiabatic index, every (sufficiently smooth) non-negative function  $\Upsilon(p)$  determines a unique (up to a constant of integration) equation of state  $\epsilon = \epsilon(p)$ . This equation of state is the solution of the ordinary differential equation

$$\frac{d\epsilon(p)}{dp} = \frac{1}{c^2} + \frac{\Upsilon(p)}{c^2}. \quad (11)$$

<sup>2</sup> The notation PB-PA is used to denote the pressure-based piecewise-analytical representation, while PB-S denotes the pressure-based spectral representation.

<sup>3</sup> The abundances of the various particles that make up neutron-star matter are determined in part by the conditions for beta equilibrium. These abundances will not have time to adjust in high frequency perturbations to their equilibrium values via these relatively slow weak interactions. The sound speed may therefore be somewhat different from that of a pure barotrope.

The solution to this equation is given by the simple quadrature:

$$\epsilon(p) = \epsilon_0 + \frac{p - p_0}{c^2} + \frac{1}{c^2} \int_{p_0}^p \Upsilon(p') dp', \quad (12)$$

where  $\epsilon_0$  is the constant of integration  $\epsilon_0 = \epsilon(p_0) \geq 0$  needed to fix the solution.

This one-to-one correspondence between non-negative  $\Upsilon(p)$  and equations of state satisfying the causality and thermodynamic stability conditions provides a natural route to constructing causal representations of these equations of state. Every non-negative  $\Upsilon(p)$  generates a causal representation. As shown in Sec. II, such functions are easy to approximate at any level of accuracy using a variety of methods, including piecewise-analytical approximations and spectral approximations.

Consider first a piecewise-analytical representation constructed by subdividing the pressure domain  $[p_0, p_{\max}]$  into  $n$  subdomains with  $p_0 < p_1 < \dots < p_{n-1} < p_{\max}$ . Figure 3 illustrates the functions  $\Upsilon(p)$  for the 27 causal nuclear-theory model equations of state in the pressure domain of interest for neutron-star interiors. This figure shows that  $\log \Upsilon(p)$  is roughly proportional to  $\log p$  for these equations of state. A reasonably good analytical representation of  $\Upsilon(p)$  in each pressure subdomain is therefore given by

$$\Upsilon(p, v_k) = \Upsilon_k \left( \frac{p}{p_k} \right)^{v_{k+1}}, \quad (13)$$

where the adjustable parameters  $\Upsilon_k$  and  $v_{k+1}$  determine its properties in each subdomain. Given this representation of  $\Upsilon(p)$ , the integral in Eq. (12) is easy to perform, and the resulting  $\epsilon(p, v_k)$  is given by

$$\begin{aligned} \epsilon(p, v_k) = & \epsilon_k + \frac{p - p_k}{c^2} \\ & + \frac{p_k \Upsilon_k}{(1 + v_{k+1})c^2} \left[ \left( \frac{p}{p_k} \right)^{1+v_{k+1}} - 1 \right] \end{aligned} \quad (14)$$

in the pressure subdomain  $p_k \leq p < p_{k+1}$ . The constants  $\Upsilon_k$  and  $\epsilon_k$  are determined iteratively by the recursion relations

$$\Upsilon_k = \Upsilon_{k-1} \left( \frac{p_k}{p_{k-1}} \right)^{v_k}, \quad (15)$$

$$\begin{aligned} \epsilon_k = & \epsilon_{k-1} + \frac{p_k - p_{k-1}}{c^2} \\ & + \frac{p_{k-1} \Upsilon_{k-1}}{(1 + v_k)c^2} \left[ \left( \frac{p_k}{p_{k-1}} \right)^{1+v_k} - 1 \right], \end{aligned} \quad (16)$$

with  $\Upsilon(p_0) = e^{v_0}$ , which enforce continuity at the pressure subdomain boundaries. The remaining constants  $v_k$  are the independent parameters that determine the equation of state in each pressure subdomain.

Spectral representations of  $\Upsilon(p)$  can also be constructed, for example by setting

$$\Upsilon(p) = \exp \left[ \sum_k v_k \Phi_k(p) \right]. \quad (17)$$

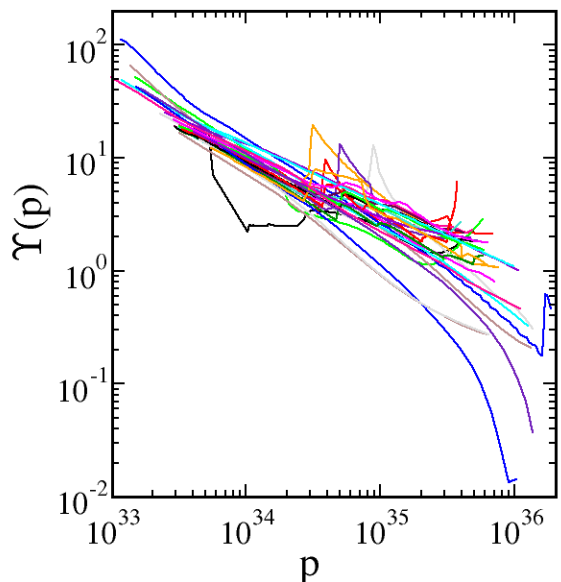


FIG. 3: Curves illustrate the sound speed function  $\Upsilon(p) = [c^2 - v^2(p)]/v^2(p)$  for 27 nuclear-theory model equations of state that satisfy the causality condition,  $\Upsilon(p) \geq 0$ , in the pressure domain of interest to neutron-star interiors.

The graphs in Fig. 3 suggest that a reasonable choice for  $\Phi_k(p)$  is  $\Phi_k(p) = [\log(p/p_0)]^k$ , the same as those used to represent  $\Gamma(p)$  in Sec. II. The associated representation of  $\epsilon(p)$  is obtained from Eq. (12):

$$\begin{aligned} \epsilon(p, v_k) = & \frac{1}{c^2} + \frac{p - p_0}{c^2} \\ & + \frac{1}{c^2} \int_{p_0}^p \exp \left\{ \sum_k v_k \left[ \log \left( \frac{p'}{p_0} \right) \right]^k \right\} dp'. \end{aligned} \quad (18)$$

Unfortunately, the integral in this expression can not be done analytically. However the integrand is very smooth, and numerical integration (e.g. using Gaussian quadrature) can be done very accurately and efficiently.

The detailed discussion of how accurately and efficiently the causal piecewise-analytical (PB-C-PA) and the causal spectral (PB-C-S) representations<sup>4</sup> work for these various equations of state is delayed to Section V. However to summarize, those tests reveal that the PB-C-PA representations are much more efficient than the non-causal PB-PA representations, while the PB-C-S representations are roughly comparable to the PB-S representations. Thus, representations that enforce causality can be used without sacrificing accuracy or efficiency.

<sup>4</sup> The notation PB-C-PA is used to denote the pressure based causal piecewise-analytical representation, while PB-C-S denotes the pressure-based causal spectral representation.

#### IV. ENTHALPY-BASED REPRESENTATIONS

The causal representations described in Sec. III are based on the pressure-based forms of the equation of state,  $\epsilon = \epsilon(p)$ . These are quite useful for many purposes, however, for some applications this standard form is not ideal. For example, a very useful form of the relativistic stellar structure equations requires the equation of state to be expressed in terms of the relativistic enthalpy,  $h$  [4]. For applications such as this,  $\epsilon = \epsilon(p)$  must be re-written as a pair of equations  $\epsilon = \epsilon(h)$  and  $p = p(h)$ , where  $h$  is defined as

$$h(p) = \int_0^p \frac{dp'}{\epsilon(p')c^2 + p'}. \quad (19)$$

The needed expressions,  $\epsilon = \epsilon(h)$  and  $p = p(h)$ , are constructed by inverting  $h = h(p)$  from Eq. (19) to obtain  $p = p(h)$ , and then composing the result with,  $\epsilon(p)$ , to obtain  $\epsilon(h) = \epsilon[p(h)]$ .

The transformations needed to construct  $\epsilon = \epsilon(h)$  and  $p = p(h)$  from  $\epsilon = \epsilon(p)$  are difficult to perform numerically in an efficient and accurate way. Therefore directly constructing parametric enthalpy-based representations is preferable. This can be done using methods analogous to those described in Secs. II and III. Enthalpy-based representations have been reported in Ref. [33] that satisfy the thermodynamic stability condition but not the causality condition. Those derivations will not be repeated here. Instead, the focus here will be on the construction of enthalpy-based causal representations.

The functions  $p(h)$  and  $\epsilon(h)$  from the enthalpy-based form of the equation of state satisfy the system of ordinary differential equations,

$$\frac{d\epsilon}{dh} = \frac{\epsilon c^2 + p}{c^2} [1 + \Upsilon(h)], \quad (20)$$

$$\frac{dp}{dh} = \epsilon c^2 + p, \quad (21)$$

which follow from the definitions of  $\Upsilon$  in Eq. (11), and  $h$  in Eq. (19). These equations imply that there is a one to one correspondence between equations of state,  $p = p(h)$  and  $\epsilon = \epsilon(h)$ , and the velocity function  $\Upsilon(h)$ . Every equation of state determines  $\Upsilon(h)$ ; and conversely, every function  $\Upsilon(h)$  determines an equation of state through Eqs. (20) and (21). Causal representations of the equation of state can therefore be constructed from representations of non-negative functions  $\Upsilon(h)$ . These representations can be constructed using either the piecewise-analytical or the spectral approaches.

Piecewise-analytical enthalpy-based representations can be constructed using the same approach as the pressure-based representations given in Secs. II and III. The first step is to divide the domain of enthalpies relevant for the high density portion of a neutron-star core,  $[h_0, h_{\max}]$ , into  $n$  subdomains with  $h_0 < h_1 < \dots < h_{n-1} < h_{\max}$ . The second step is to choose analytical functions  $\Upsilon(h, v_k)$  to approximate  $\Upsilon(h)$  in each subdomain. The challenge is to find analytical functions that

are reasonably good approximations in each subdomain, and that are simple enough to allow Eqs. (20) and (21) to be solved analytically for  $\epsilon(h, v_k)$  and  $p(h, v_k)$ . Figure 4 shows  $\Upsilon(h)$  in the relevant range of  $h$  for 27 causal nuclear-theory model equations of state. These graphs show that  $\log \Upsilon$  is more or less proportional to  $-\log h$  for these equations of state. This fact, together with the need to have simple analytical functions having analytical integrals, leads to the following choice for  $\Upsilon(h, v_k)$ ,

$$\Upsilon(h, v_k) = \frac{v_k + 2(h_{k+1} - h)}{h}, \quad (22)$$

in the subdomain  $h_k \leq h < h_{k+1}$ . These functions are non-negative within each subdomain so long as non-negative adjustable parameters are chosen,  $v_k \geq 0$ .

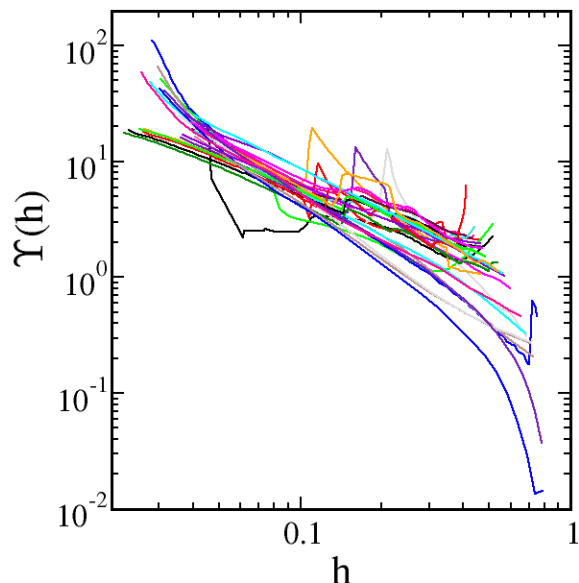


FIG. 4: Curves illustrate the sound speed function  $\Upsilon(h)$  for 27 nuclear-theory model equations of state that satisfy the causality condition,  $\Upsilon(h) \geq 0$ , in the enthalpy domain of interest to neutron-star interiors.

The piecewise-analytical representation of the equation of state,  $\epsilon(h, v_k)$  and  $p(h, v_k)$ , that corresponds to the  $\Upsilon(h, v_k)$  given in Eq. (22) is determined by solving Eqs. (20) and (21). The general solution to these equations can be reduced to quadrature:

$$p(h) = p_0 + (\epsilon_0 c^2 + p_0) \int_{h_0}^h \mu(h') dh', \quad (23)$$

$$\epsilon(h) = -p(h) c^{-2} + (\epsilon_0 + p_0 c^{-2}) \mu(h), \quad (24)$$

where  $\mu(h)$  is defined as,

$$\mu(h) = \exp \left\{ \int_{h_0}^h [2 + \Upsilon(h')] dh' \right\}. \quad (25)$$

The constants  $p_0$  and  $\epsilon_0$  are defined by  $p_0 = p(h_0) \geq 0$  and  $\epsilon_0 = \epsilon(h_0) \geq 0$  respectively. Inserting the expression

for  $\Upsilon(h, v_k)$  from Eq. (22) into these integrals gives the following expressions for the equation of state,

$$p(h, v_k) = p_k + \frac{(\epsilon_k c^2 + p_k) h_k}{v_k + 2h_{k+1} + 1} \left[ \left( \frac{h}{h_k} \right)^{v_k + 2h_{k+1} + 1} - 1 \right], \quad (26)$$

$$\epsilon(h, v_k) = -p(h, v_k) c^{-2} + (\epsilon_k + p_k c^{-2}) \left( \frac{h}{h_k} \right)^{v_k + 2h_{k+1}}, \quad (27)$$

in the subdomain  $h_k \leq h < h_{k+1}$ . The constants  $p_k = p(h_k, v_k)$  and  $\epsilon_k = \epsilon(h_k, v_k)$  are determined from the recursion relations,

$$p_{k+1} = p_k + \frac{(\epsilon_k c^2 + p_k) h_k}{v_k + 2h_{k+1} + 1} \left[ \left( \frac{h_{k+1}}{h_k} \right)^{v_k + 2h_{k+1} + 1} - 1 \right], \quad (28)$$

$$\epsilon_{k+1} = -p_{k+1} c^{-2} + (\epsilon_k + p_k c^{-2}) \left( \frac{h_{k+1}}{h_k} \right)^{v_k + 2h_{k+1}}. \quad (29)$$

Causal enthalpy-based representations of the equation of state can also be constructed using spectral methods. The basic idea is to represent the velocity function  $\Upsilon(h)$  as a spectral expansion:

$$\Upsilon(h, v_k) = \exp \left[ \sum_k v_k \Phi_k(h) \right], \quad (30)$$

where the  $\Phi_k(h)$  is any complete set of basis functions on the domain  $[h_0, h_{\max}]$ . Figure 4 shows that the  $\Upsilon(h)$  for the collection of 27 causal nuclear-theory model equations of state are fairly simple functions of  $\log h$ . Therefore, following the approach used in Ref. [33] we take the spectral basis functions  $\Phi_k(h)$  to be  $\Phi_k(h) = [\log(h/h_0)]^k$ . The expression for  $\Upsilon(h, v_k)$  then becomes:

$$\Upsilon(h, v_k) = \exp \left\{ \sum_k v_k \left[ \log \left( \frac{h}{h_0} \right) \right]^k \right\}. \quad (31)$$

While the quadratures in Eqs. (23) and (25) can not be done analytically for the spectral expansion defined in Eqs. (31), they can be done numerically very efficiently and accurately using Gaussian quadrature.

The detailed discussion of how accurately and efficiently the enthalpy-based causal piecewise-analytical (HB-C-PA) and the causal spectral (HB-C-S) representations<sup>5</sup> work for these various equations of state is delayed to Section V. However to summarize, those tests reveal

that the HB-C-PA representations are roughly comparable to the non-causal PB-PA representations (somewhat better for  $n \geq 4$ , somewhat worse for  $n \leq 3$ ), while the HB-C-S representations are roughly comparable to the HB-S representation. Thus enthalpy-based representations that enforce causality can be used without sacrificing accuracy or efficiency.

## V. TESTING THE REPRESENTATIONS

This section presents numerical tests of the accuracy and efficiency of the various parametric representations of neutron-star equations of state described in Secs. II–IV. Representations of 27 nuclear-theory model neutron-star equation of state models are constructed and then compared with the originals to measure their accuracy and efficiency. The 27 model equations of state used in these tests are the causality satisfying subset of the collection of 34 nuclear-theory based models used by Read, et al. [2] in their study of the piecewise-polytropic representations. The particular equations of state excluded from their collection are APR2, APR3, APR4, WFF1, WFF2 ENG, and ALF1, each of which violates the causality condition  $dp/d\epsilon \leq c^2$  for some range of densities.

Each of the nuclear-theory model equations of state consists of a table of energy-density pressure pairs:  $\{\epsilon_i, p_i\}$  for  $1 \leq i \leq N$ . A parametric representation of one of these equations of state consists of a function  $\epsilon(p, v_k)$  that gives the energy density as a function of the pressure, and also the parameters  $v_k$  for  $1 \leq k \leq n$ . The accuracy of a particular representation is determined by evaluating the dimensionless error residual  $\Delta_n(v_k)$ , defined by

$$\Delta_n^2(v_k) = \sum_{i=1}^N \frac{1}{N} \left\{ \log \left[ \frac{\epsilon(p_i, v_k)}{\epsilon_i} \right] \right\}^2. \quad (32)$$

The optimal choice of the parameters  $v_k$  to represent a particular equation of state  $\{\epsilon_i, p_i\}$  is obtained by minimizing  $\Delta_n(v_k)$  with respect to variations in each of the parameters  $v_k$ . This minimization is carried out numerically for these tests using the Levenberg-Marquardt method [34]. The minimum values of  $\Delta_n$  obtained in this way are illustrated for the pressure-based causal piecewise-analytical (PB-C-PA) representation in Fig. 5 and the pressure-based causal spectral (PB-C-S) representation in Fig. 6. Each of the 27 curves in these figures represents the residual  $\Delta_n$  as a function of the number of parameters  $n$  for one of the causal nuclear-theory model equations of state. These curves generally show convergence, i.e.  $\Delta_n \geq \Delta_{n+1}$ , thus showing that the minimization methods used in these tests are effective. As expected, the different curves converge at different rates for the various equations of state, depending on how complicated the structure of the function  $\Upsilon(p)$  is for each case. Also as expected, the average residuals  $\Delta_n$  for the spectral representations in Fig. 6 are smaller (for given value

<sup>5</sup> The notation HB-C-PA is used to denote the enthalpy-based causal piecewise-analytical representation, while HB-C-S denotes the enthalpy-based causal spectral representation.

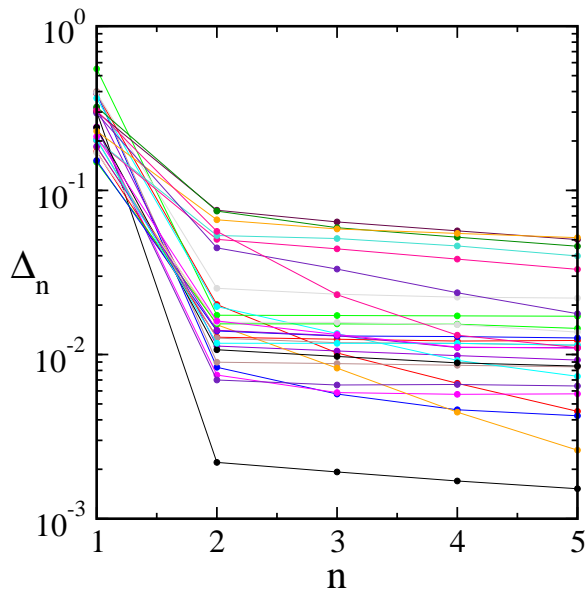


FIG. 5: Residuals  $\Delta_n$  are illustrated as functions of  $n$  (the number of parameters  $v_k$  used) for the pressure-based causal piecewise-analytical (PB-C-PA) representations of 27 causal nuclear-theory model equations of state.

of  $n$ ) than their counterparts for the piecewise-analytical representations in Fig. 5.

Figure 7 illustrates the residuals  $\Delta_n$  for the enthalpy-based causal spectral (HB-C-S) representation discussed in Sec. IV. The residuals in this case are computed in much the same way as those for the pressure-based representations. The only difference is the  $\epsilon(h_i, v_k)$  that appears in error residual

$$\Delta_n^2(v_k) = \sum_{i=1}^N \frac{1}{N} \left\{ \log \left[ \frac{\epsilon(h_i, v_k)}{\epsilon_i} \right] \right\}^2 \quad (33)$$

now depends on  $h_i$ , the enthalpy corresponding to the point  $\{\epsilon_i, p_i\}$  for the particular equation of state. Comparing Figs. 6 and 7 shows that the accuracy and efficiency of the enthalpy-based spectral representations are comparable to their pressure-based counterparts.

Representations of the 27 causal nuclear-theory model equations of state were constructed in this way for each of the seven different methods described in Secs. II–IV. In particular representations were constructed for the pressure-based piecewise-analytical (PB-PA) and the pressure-based spectral (PB-S) representations described in Sec. II, the pressure-based causal piecewise-analytical (PB-C-PA) and the pressure-based causal spectral (PB-C-S) representations described in Sec. III, and finally for the enthalpy-based spectral (HB-S), the enthalpy-based causal piecewise-analytical (HB-C-PA), and the enthalpy-based causal spectral (HB-C-S) representations discussed in Sec. IV. Some of these representations (PB-PA, PB-S, and HB-S) had been discussed previously in the literature (see e.g. Ref. [33]) so detailed convergence

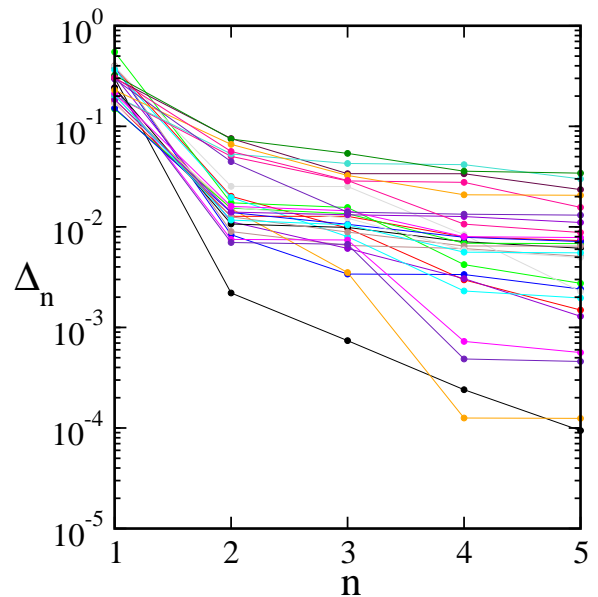


FIG. 6: Residuals  $\Delta_n$  are illustrated as functions of  $n$  (the number of parameters  $v_k$  used) for the pressure-based causal spectral (PB-C-S) representations of 27 causal nuclear-theory model equations of state.

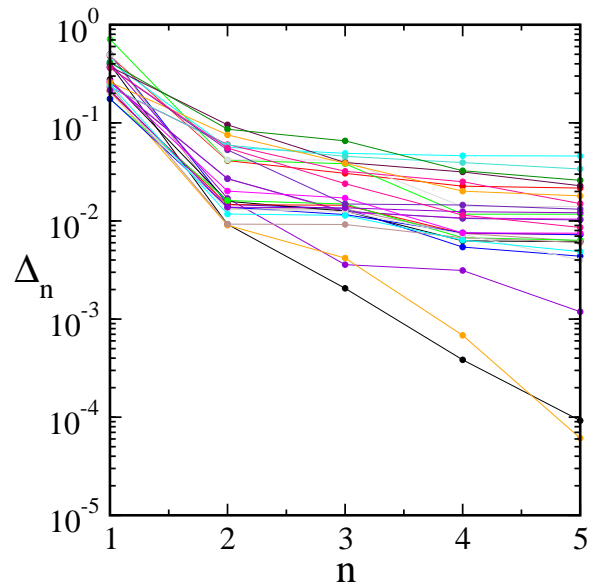


FIG. 7: Residuals  $\Delta_n$  are illustrated as functions of  $n$  (the number of parameters  $v_k$  used) for the enthalpy-based causal spectral (HB-C-S) representations of 27 causal nuclear-theory model equations of state.

plots are not given here for those cases. Instead the average values of  $\Delta_n$  (where the averages are taken over the 27 causal equation of state models) are illustrated in Fig. 8. This figure shows clearly that the spectral representations (with circular data points and colored blue) are more efficient on average than the piecewise-analytical representations (with square data points and

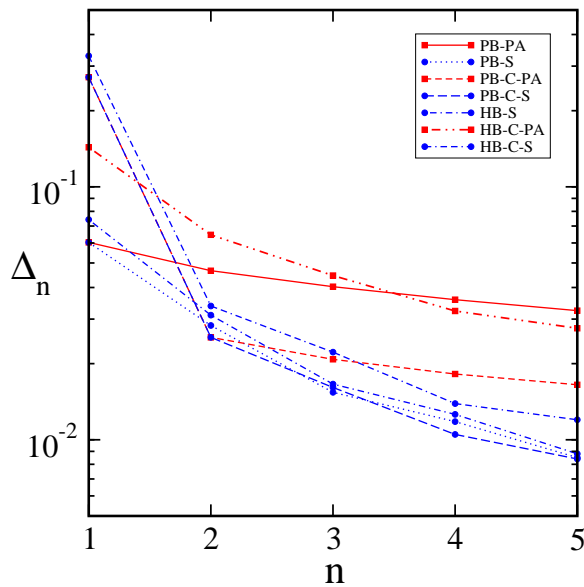


FIG. 8: Convergence of the average residuals  $\Delta_n$  is illustrated for the seven different representations studied here. Piecewise-analytical representations are shown with square data points (and colored red), while the spectral representations are shown with round data points (and colored blue).

colored red). This figure also shows that the pressure-based causal piecewise-analytical representation (PB-C-PA) is much more efficient on average than either of the other two piecewise-analytical representations (PB-PA and HB-C-PA) considered here. And, this figure reveals that all the spectral representations are more or less comparable, with the pressure-based causal spectral (PB-C-S) representation being slightly more efficient than the others studied here.

## VI. DISCUSSION

The graphs in Figs. 5–7 illustrate the convergence of the error residuals  $\Delta_n$  as the number of parameters  $n$  is increased for three new causal representations of neutron-star equations of state presented here. Each curve in each figure represents one of the 27 causal nuclear-physics model equations of state included in this study. These graphs show that there is a fairly large range of convergence rates for these representations among the different equation of state models. The differences in convergence rates arise from the differences in the equation of state functions  $\Upsilon(p)$  or  $\Upsilon(h)$  illustrated in Figs. 3 and 4. Those equations of state with  $\Upsilon$  having more structure, e.g. including discontinuities from phase transitions, have representations that converge more slowly than smooth equations of states having less structure. These graphs also show that even the most difficult cases studied here (i.e. those with strong phase transitions) have errors  $\Delta_n < 0.1$ , for  $n \geq 2$ , and  $\Delta_5 \leq 0.05$ . These graphs also show that the spectral representations con-

verge more rapidly than the piecewise analytical representations, even for the more difficult cases with phase transitions. The relationship between the equation of state structure and the efficiency of representations was studied in some detail in Ref. [33]. That earlier work focused on non-causal representations, however, the relationship between the structure of the equation of state and the convergence rate of these types of representations is the same in the cases studied here.

The most widely used representation of the neutron-star equation of state (at the present time) is the piecewise-polytropic representation [2, 31, 32]. The most carefully studied version of this representation uses four adjustable parameters [2], whose best-fit representation has an error residual  $\Delta_4 = 0.0383$  when averaged over 34 nuclear-theory model equations of state [33]. While this representation is essentially equivalent to the pressure-based piecewise-analytical representation (PB-PA) discussed in Sec. II, there are some minor differences. The solid curve in Fig. 8 shows the convergence of the average residuals  $\Delta_n$  for the PB-PA representation, which has the value  $\Delta_4 = 0.0358$  for the four-parameter case. These results differ slightly from the earlier work for two reasons. First, the collection of 27 causal nuclear-theory model equations of state used in the tests here is a subset of the 34 equations of state used in the earlier studies. And second, the four parameters adjusted in the earlier study to obtain the best-fit representation are the three subdomain adiabatic index parameters,  $\gamma_1$ ,  $\gamma_2$  and  $\gamma_3$ , plus the location of the first pressure subdomain boundary  $p_1$ . In the present work the locations of the subdomain boundaries are uniformly spaced and fixed, while the  $n$  adiabatic index parameters  $\gamma_k$  for  $k = 1, \dots, n$  are adjusted to obtain the best fits.

One notable feature of the results of the convergence tests performed here is how slowly  $\Delta_n$  decreases for the PB-PA representation as the number of parameters is increased. Figure 8 shows that while the residual  $\Delta_1$  for the one parameter version of PB-PA is actually the smallest, its residuals  $\Delta_n$  become the largest when  $n \geq 4$ . Almost all of the other representations (except HB-C-PA) have smaller two parameter residuals  $\Delta_2$  than  $\Delta_4$  for the widely used four-parameter version of PB-PA. The PB-PA representation is therefore (along with HB-C-PA) the least accurate and efficient of the representations studied here. These representations therefore fail to satisfy the basic Principle #3, efficiency, from the discussion in Sec. I. The PB-C-PA representation is much more efficient than PB-PA, and has the added advantage of automatically enforcing causality. Therefore if a piecewise-analytical representation is desired (e.g. because it is easier to code up, or because it is more efficient to use numerically than the spectral representations) the PB-C-PA representation described in Sec. III is probably a better choice than PB-PA. The most efficient representations, however, are the spectral representations, PB-S, PB-C-S, HB-S and HB-C-S. The most efficient of these is the pressure-based causal spectral representation PB-

C-S. This representation also satisfies Principles #1 and #2 of the general discussion in Sec. I. This study therefore suggests that the PB-C-S representation is probably the best choice for a representation of the neutron-star equation of state available at this time.

### Acknowledgments

I thank Steve Lewis and Fridolin Weber for helpful comments and suggestions on an early draft of this pa-

per. This research was supported in part by grants PHY-1604244 and DMS-1620366 from the National Science Foundation.

- 
- [1] B. Friman, C. Höhne, J. Knoll, S. Luepold, J. Randrup, R. Rapp, and P. Senger, eds., *The CBM Physics Book*, vol. 814 of *Lecture Notes in Physics* (Springer-Verlag, 2011).
- [2] J. S. Read, B. D. Lackey, B. J. Owen, and J. L. Friedman, *Phys. Rev. D* **79**, 124032 (2009).
- [3] J. R. Oppenheimer and G. M. Volkoff, *Phys. Rev.* **55**, 374 (1939).
- [4] L. Lindblom, *Astrophys. J.* **398**, 569 (1992).
- [5] L. Lindblom, *AIP Conference Proceedings* **1577**, 153 (2014).
- [6] W. D. Arnett and R. L. Bowers, *Ap. J. Suppl. Ser.* **33**, 415 (1977).
- [7] J. M. Lattimer and M. Prakash, *Phys. Rept.* **442**, 109 (2007).
- [8] F. Özel, T. Güver, and D. Psaltis, *Astrophys. J.* **693**, 1775 (2009).
- [9] A. W. Steiner, J. M. Lattimer, and E. F. Brown, *Astrophys. J.* **722**, 33 (2010).
- [10] T. Güver, F. Özel, A. Cabrera-Lavers, and P. Wroblewski, *Astrophys. J.* **712**, 964 (2010).
- [11] T. Güver, P. Wroblewski, L. Camarota, and F. Özel, *Astrophys. J.* **719**, 1807 (2010).
- [12] A. W. Steiner, J. M. Lattimer, and E. F. Brown, *Astrophys. J.* **765**, L5 (2013).
- [13] D. K. Galloway and N. Lampe, *Astrophys. J.* **747**, 75 (2012).
- [14] T. Güver, D. Psaltis, and F. Özel, *Astrophys. J.* **747**, 76 (2012).
- [15] T. Güver, F. Özel, and D. Psaltis, *Astrophys. J.* **747**, 77 (2012).
- [16] M. Zamfir, A. Cumming, and D. K. Galloway, *Astrophys. J.* **749**, 69 (2012).
- [17] F. Özel, A. Gould, and T. Güver, *Astrophys. J.* **748**, 5 (2012).
- [18] T. Güver and F. Özel, *Astrophys. J.* **765**, L1 (2013).
- [19] J. M. Lattimer and A. W. Steiner, *Astrophys. J.* **784**, 123 (2015).
- [20] Nättilä, M. C. Miller, A. W. Steiner, J. J. E. Kajava, V. F. Suleimanov, and J. Poutanen, *Astron. Astrophys.* **608**, A31 (2017).
- [21] A. Steiner, C. Heinke, S. Bogdanov, C. Li, W. Ho, A. Bahramian, and S. Han, *Mon. Not. Roy. Astr. Soc.* **476**, 421 (2018).
- [22] A. W. Shaw, C. O. Heinke, A. W. Steiner, H. N. C. S. Campana, W. C. G. Ho, P. M. Lugger, and M. Servillat, *Mon. Not. Roy. Astr. Soc.* (2018), submitted.
- [23] L. Lindblom and N. M. Indik, *Phys. Rev. D* **86**, 084003 (2012).
- [24] L. Lindblom and N. M. Indik, *Phys. Rev. D* **89**, 064003 (2014).
- [25] T. Abdelsalhin, A. Maselli, and V. Ferrari (2017), arXiv:1712.01303.
- [26] F. Özel, G. Baym, and T. Guver, *Phys. Rev. D* **82**, 101301 (2010).
- [27] F. Özel, D. Psaltis, T. Güver, G. Baym, C. Heinke, and S. Guillot, *Astrophys. J.* **820**, 28 (2016).
- [28] F. Özel and P. Freire, *Ann. Rev. Astron. and Astroph.* **54**, 401 (2016).
- [29] C. A. Raithel, F. Özel, and D. Psaltis, *Astrophys. J.* **831**, 44 (2016).
- [30] C. A. Raithel, F. Özel, and D. Psaltis, *Astrophys. J.* **844**, 156 (2016).
- [31] C. Vuille (1995), unpublished; arXiv:0812.3828.
- [32] C. Vuille and J. Ipser, in *Eighth Canadian Conference on General Relativity and Relativistic Astrophysics*, edited by C. P. Burgess and R. C. Meyers (1999), vol. 493 of *AIP Conference Proceedings*, p. 60.
- [33] L. Lindblom, *Phys. Rev. D* **82**, 103011 (2010).
- [34] W. H. Press, S. A. Teukolsky, W. T. Vetterling, and B. P. Flannery, *Numerical Recipes in FORTRAN* (Cambridge University Press, Cambridge, England, 1992), 2nd ed.